

## Polymerization/Depolymerization-Induced Self-Assembly under Coupled Equilibria of Polymerization with Self-Assembly

Jiyun Nam, Changsu Yoo, and Myungeun Seo\*

Cite This: *J. Am. Chem. Soc.* 2024, 146, 13854–13861

Read Online

ACCESS |



Metrics &amp; More

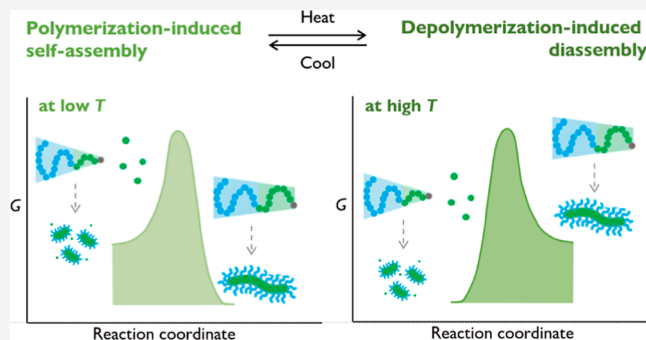


Article Recommendations



Supporting Information

**ABSTRACT:** Depolymerization breaks down polymer chains into monomers like unthreading beads, attracting more attention from a sustainability standpoint. When polymerization reaches equilibrium, polymerization and depolymerization can reversibly proceed by decreasing and increasing the temperature. Here, we demonstrate that such dynamic control of a growing polymer chain in a selective solvent can spontaneously modulate the self-assembly of block copolymer micellar nano-objects. Compared to polymerization-induced self-assembly (PISA), where irreversible growth of a solvophobic polymer block from the end of a solvophilic polymer causes micellization, polymerization/depolymerization-induced self-assembly presented in this study allows us to reversibly regulate the packing parameter of the forming block copolymer and thus induce reversible morphological transitions of the nano-objects by temperature swing. Under the coupled equilibria of polymerization with self-assembly, we found that demixing of the growing polymer block in a more selective solvent entropically facilitates depolymerization at a substantially lower temperature. Taking ring-opening polymerization of  $\delta$ -valerolactone initiated from the hydroxyl-terminated poly(ethylene oxide) as a model system, we show that polymerization/depolymerization/repolymerization leads to reversible morphological transitions, such as rod–sphere–rod and fiber–rod–fiber, during the heating and cooling cycle and accompanied by changes in macroscopic properties such as viscosity, suggesting their potential as dynamic soft materials.



## INTRODUCTION

In the membrane-bounded compartment nature of a cell, fibrous filaments dynamically grow 1D nanostructures via polymerization equilibrium.<sup>1,2</sup> The inherent dissociation of the actin polymer into monomer, regulated by polymerization equilibrium, allows for the sustainable restructuring of the actin filament from the recyclable monomers.<sup>3,4</sup> Such an “equilibrium polymerization” is an appealing concept toward a sustainable polymer economy by breaking down polymer chains back to reusable monomer feedstock and rebuilding them on demand.<sup>5–8</sup>

In the case of ring-opening polymerization (ROP) of a small-sized heterocyclic monomer (4–7 membered rings), polymerization thermodynamics is governed by a balance of a negative enthalpy change ( $\Delta H_p$ ) with a negative entropy change ( $\Delta S_p$ ), corresponding to the release of the monomer ring strain and the increased order of the system, respectively.<sup>9,10</sup> Upon heating above the ceiling temperature ( $T_c$ ), where the polymerization rate is equal to that of depolymerization, ring-closing depolymerization dominates and reverses the chain growth polymerization generating pure monomer feedstock as the entropic penalty prevails over the enthalpic gain.<sup>11,12</sup> Examples of monomer recovery from polymeric materials have been reported as a means of chemical recycling.<sup>13–15</sup> However, the effect of reversible polymer-

ization/depolymerization on the structure of self-assembled polymeric materials has not been investigated. Inspired by actin polymerization, we envisioned that growing and chopping off polymer chains, joined by covalent bonds, would add a unique dynamic feature in manipulating polymer nanostructures typically composed of presynthesized, static polymer building blocks and organized via noncovalent interactions.

While relying on irreversible polymerization, polymerization-induced nanostructuring techniques such as polymerization-induced self-assembly (PISA)<sup>16,17</sup> and polymerization-induced microphase separation (PIMS)<sup>18,19</sup> are powerful strategies that dynamically combine polymerization with block polymer-based nanostructuring. By choosing a monomer soluble in the polymerization mixture, but its polymer is incompatible with the medium, polymerization produces a diblock copolymer that spontaneously self-assembles at a critical conversion to

Received: January 14, 2024

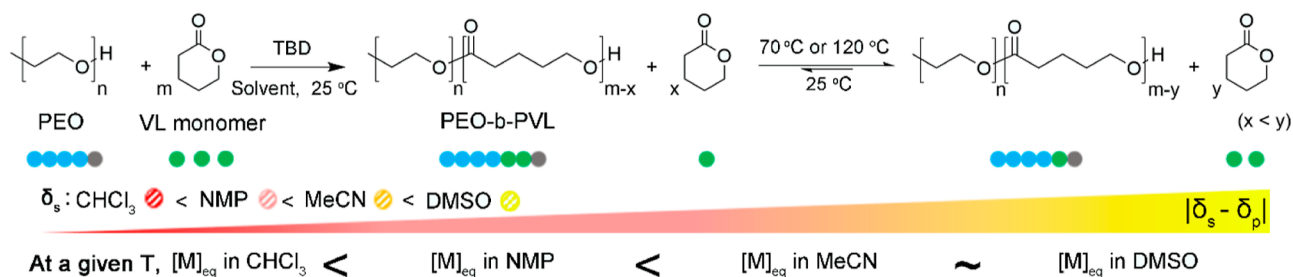
Revised: April 23, 2024

Accepted: April 25, 2024

Published: May 8, 2024



## a. Coupling of polymerization and self-assembly equilibria



## b. Polymerization/depolymerization-induced self-assembly

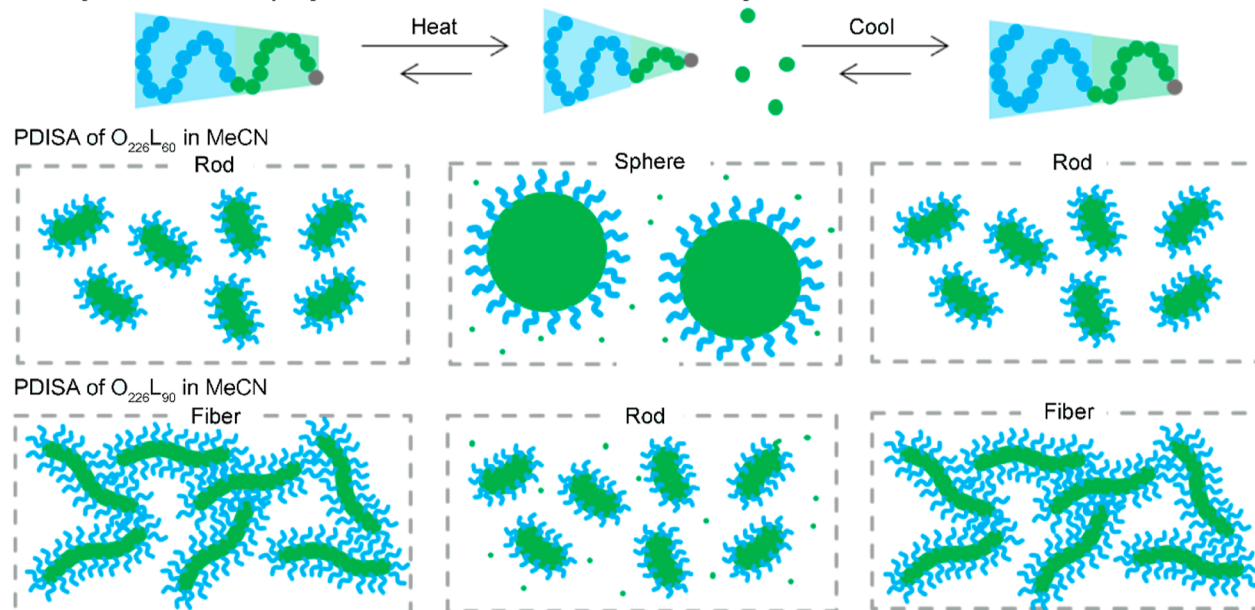


**Figure 1.** Schematic illustrations of polymerization/depolymerization-induced self-assembly under coupled equilibria of polymerization and self-assembly. (a) Coupling of polymerization and self-assembly equilibria of VL when the chain is extended from PEO using TBD in various reaction media. The solvophobic interaction between the solvent and the PVL block is denoted by arrows. (b) Polymerization/depolymerization-induced self-assembly of OL in MeCN.

minimize the contact of the growing chain to the medium. Versatile nano-objects such as spherical and worm-like micelles have been produced by PISA operated in a selective solvent with morphological transitions as a function of conversion.<sup>20,21</sup> Utilizing reversible phase transitions such as low and upper critical solution temperatures enabled further control over morphologies.<sup>22–25</sup> These examples are all based on one-way irreversible polymerization where the polymer becomes static once produced and the reversible feature stems from noncovalent interaction. While PISA examples based on ROP of alicyclic monomers have been reported, efforts to utilize the depolymerization behavior have been missing.<sup>26,27</sup>

Herein, we present the polymerization/depolymerization-induced self-assembly (PDISA) controlled by the polymerization equilibrium, as depicted in Figure 1. As the equilibrium monomer concentration is set by the temperature, we demonstrate that polymerization- and depolymerization-

dominant states can be reversibly switched by lowering and elevating the temperature of the polymerization mixture. The resulting change in the chain length of the solvophobic block regulates the packing parameter of the diblock copolymer and induces morphological transitions much more drastically than static PISA. No phase transition in the absence of the polymerization catalyst corroborates the depolymerization-induced phase transition mechanism. The key is to choose the right solvent that lowers  $T_c$ , so the polymerization equilibrium can be readily controlled by the temperature change. Our findings suggest that the free-energy change upon micellization affects the thermodynamic parameters of polymerization. Under the coupled equilibria of polymerization with self-assembly, the increasing unfavorable entropic contribution in the more selective solvent shifts the polymerization equilibrium toward depolymerization. We believe PDISA will further enrich the PISA toolbox and ultimately open a route to

dynamic soft materials based on equilibrium polymerization principles inspired by nature.

## RESULTS AND DISCUSSION

We first tested the effect of the solvent selectivity on  $T_c$ . We chose  $\delta$ -valerolactone (VL), a six-membered cyclic ester, as the monomer because of its relatively low  $T_c$  (155 °C at 1 M, toluene).<sup>28</sup> With the hydroxyl-terminated poly(ethylene oxide) (PEO) with a number-average molar mass ( $M_n$ ) of 10 kg mol<sup>-1</sup> as a macroinitiator and triazabicyclodecene (TBD) as a catalyst, we performed ROP of VL in several solvents with different polarities at 25 °C (see the [Supporting Information](#) for details). We used a Hansen solubility parameter of the solvent ( $\delta_s$ ) to predict its selectivity to PVL: chloroform ( $\text{CHCl}_3$ ,  $\delta_{\text{CHCl}_3} = 20.2 \text{ MPa}^{1/2}$ ),<sup>29</sup> *N*-methylpyrrolidone (NMP,  $\delta_{\text{NMP}} = 23.0 \text{ MPa}^{1/2}$ ),<sup>30</sup> acetonitrile (MeCN,  $\delta_{\text{MeCN}} = 24.4 \text{ MPa}^{1/2}$ ),<sup>31</sup> and dimethyl sulfoxide (DMSO,  $\delta_{\text{DMSO}} = 26.7 \text{ MPa}^{1/2}$ )<sup>32</sup> were selected as the reaction solvents. We estimated the solubility parameter of the VL monomer ( $\delta_m$ ) and PVL ( $\delta_p$ ) as the same as  $\gamma$ -valerolactone (24.2 MPa<sup>1/2</sup>)<sup>33</sup> and poly(3-hydroxyethanoate) (19.5 MPa<sup>1/2</sup>),<sup>34</sup> respectively, due to their constitutional isomeric structure. We confirmed that PVL was highly soluble in  $\text{CHCl}_3$ , but its solubility became poorer with the increasing  $|\delta_s - \delta_p|$ . The VL monomer and PEO ( $\delta_{\text{PEO}} = 22.8 \text{ MPa}^{1/2}$ )<sup>35</sup> were soluble in all solvents used in this study. DMSO was an exception where heat had to be applied to dissolve PEO.

Polymerization at 25 °C successfully produced PEO-*b*-PVL. <sup>1</sup>H NMR spectra of the polymerization mixtures showed the methylene proton adjacent to the estereal oxygen in the PVL repeating unit becomes broader with the increasing  $|\delta_s - \delta_p|$ , suggesting that the PVL block would be more segregated from the reaction medium via the PISA process ([Figures S1–S3](#)). We confirmed that micellar nano-objects were produced in MeCN and DMSO by transmission electron microscopy (TEM), while the polymerization mixtures in  $\text{CHCl}_3$  and NMP were relatively homogeneous ([Figure S4](#)). Rodlike and spherical micellar morphologies were identified from the polymerization mixtures in MeCN and DMSO, respectively. Dynamic light scattering (DLS) data were also consistent with the micelle formation in MeCN and DMSO ([Figure S5](#)). We denote the polymerization systems  $\text{O}_x\text{L}_y$ , henceforth, where  $x$  and  $y$  represent the degree of polymerization ( $\text{DP}_n$ ) of PEO and [VL]/[PEO] in the polymerization mixture.

Conversion of VL was strongly affected by solvent selectivity. With  $\text{O}_{226}\text{L}_{60}$  at 25 °C, the highest conversion of 82% was achieved in  $\text{CHCl}_3$ . The conversion decreased with the increasing  $|\delta_s - \delta_p|$  and reached 67% when DMSO was used, suggesting that the polymerization equilibrium is coupled with PISA. We examined equilibrium monomer concentrations ( $[\text{M}]_{\text{eq}}$ ) by performing polymerizations at different temperatures with the initial monomer concentration ( $[\text{M}]_0$ ) of 1 M ([Figures S6–S11](#)). [Figure 2a](#) shows  $[\text{M}]_{\text{eq}}$  plotted as a function of the inverse absolute temperature. An increase in  $[\text{M}]_{\text{eq}}$  following the order  $[\text{M}]_{\text{eq,CHCl}_3} < [\text{M}]_{\text{eq,NMP}} < [\text{M}]_{\text{eq,MeCN}} \sim [\text{M}]_{\text{eq,DMSO}}$  indicates that the more incompatible solvent favors depolymerization ([Table S1](#)). We extracted the apparent  $\Delta H$  and  $\Delta S$  values associated with the polymerization from the plots according to the Dainton–Ivin equation<sup>36</sup> and plotted them as a function of  $\delta_s$  in [Figure 2b](#) ([Table S2](#)).

The extracted thermodynamic parameters for the VL polymerization in  $\text{CHCl}_3$  were comparable to the reported

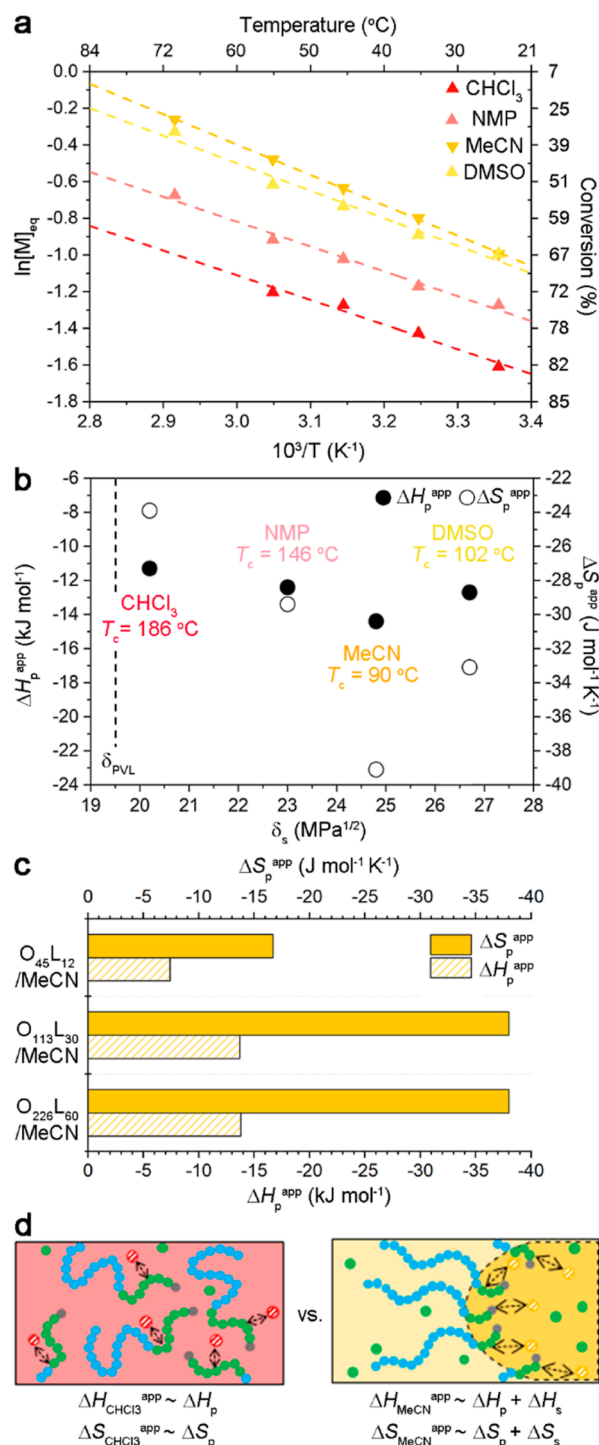


**Figure 2.** (a) Polymerization thermodynamics in different solvents. All reactions were carried out at  $[\text{VL}]_0 = 1.0 \text{ M}$ ,  $[\text{TBD}]_0 = 33 \text{ mM}$ , and  $[\text{PEO}]_0 = 17 \text{ mM}$ . (b)  $\Delta H_p^{\text{app}}$  and  $\Delta S_p^{\text{app}}$  of the  $\text{O}_{226}\text{L}_{60}$  as a function of  $\delta_s$ . (c)  $\Delta H_p^{\text{app}}$  and  $\Delta S_p^{\text{app}}$  in MeCN as a function of the chain length. (d) Schematic description for the effect of solvent selectivity on the polymerization equilibrium.  $\Delta H_p$  and  $\Delta S_p$  denote changes in enthalpy and entropy upon VL polymerization in a homogeneous mixture.  $\Delta H_s$  and  $\Delta S_s$  represent changes in enthalpy and entropy upon segregation of the PVL block via micellization.

values obtained in toluene ( $\Delta H_p^{\text{app}} = -12.2 \text{ kJ mol}^{-1}$ ,  $\Delta S_p^{\text{app}} = -28.6 \text{ J mol}^{-1} \text{ K}^{-1}$ ),<sup>28</sup> which is also a good solvent to PVL. While changing the solvent to NMP and MeCN increased the magnitude of both  $\Delta H_p^{\text{app}}$  and  $\Delta S_p^{\text{app}}$ , the outweighing



entropic contribution to the polymerization was apparent by the 56% growth in  $|\Delta S_p^{\text{app}}|$  in MeCN, compared to  $\text{CHCl}_3$ , over the 23% increase in  $|\Delta H_p^{\text{app}}|$ . As a result, a substantial reduction in  $T_c$  from 186 °C in  $\text{CHCl}_3$  to 90 °C in MeCN was found.

The entropy-driven depression of  $T_c$  is in contrast to the previous studies performed in the good solvent regime, where a solvent with smaller  $|\delta_s - \delta_m|$  or larger  $|\delta_s - \delta_p|$  decreases the enthalpic gain leading to the reduction in  $T_c$ .<sup>37,38</sup> We postulate that spontaneous micelle formation during polymerization in the selective solvent would segregate the PVL block from the solution. This unmixing creates an additional enthalpic gain (by avoiding unfavorable contact of PVL to the solvent) and also an entropic loss (by reducing the number of possible combinations for arranging PVL chains and the solvent molecules).<sup>39,40</sup> We examined the polymerization equilibrium in MeCN with shorter PEOs at the fixed  $[M]_0$  of 1 M and the identical  $[\text{PEO}]/[\text{VL}]$  ratio (1:60) to investigate the effect of micellization further and summarized the  $\Delta H_p^{\text{app}}$  and  $\Delta S_p^{\text{app}}$  values in Figure 2c (Table S2 and Figures S10–S14). While polymerizations with long- and medium-sized PEOs ( $\text{O}_{226}\text{L}_{60}$  and  $\text{O}_{113}\text{L}_{30}$ , respectively) showed essentially identical thermodynamics, both  $|\Delta H_p^{\text{app}}|$  and  $|\Delta S_p^{\text{app}}|$  values decreased drastically when a short PEO ( $\text{O}_{45}\text{L}_{12}$ ) was used. As expected, TEM and DLS data showed that micelles were formed in  $\text{O}_{226}\text{L}_{60}$  and  $\text{O}_{113}\text{L}_{30}$  following the PISA process, but no micellization occurred in  $\text{O}_{45}\text{L}_{12}$ , presumably because of the large entropic penalty for the demixing of the short PVL block in solution (Figures S15 and S16). Overall, all data are consistent with our interpretation that the additional entropic loss caused by micellization shifts the polymerization equilibrium toward depolymerization. Thus, PISA in the more selective solvent entropically facilitates depolymerization, as we schematically illustrated in Figure 2d. DMSO deviates from this trend, presumably because the relatively lower solubility of PEO in DMSO would not promote micelle formation. Because we have not seen a noticeable deviation in the monomer concentration in the polymerization mixture by  $^1\text{H}$  NMR spectroscopy (Figures S1–S3), we posit that demixing of the PVL block, not accumulation of the VL monomer in the micellar core, is mainly responsible for the entropy loss. We also note that segregation by micelle formation is distinct from precipitation by crystallization, which shifts the polymerization equilibrium to drive polymerization further, as the VL monomer can still access the propagation center at the chain end in the micellar core and keep the equilibrium with the PVL block.<sup>41</sup>

The considerably lower  $T_c$  in the VL polymerization in MeCN allows us to readily control the polymerization- and depolymerization-dominant states in the PDISA process by switching the polymerization temperature from 25 to 70 °C. We set 70 °C as the upper bound to maximize depolymerization but avoid vaporization of MeCN (its boiling point is 82 °C). We indicate the polymerization temperature ( $z$ ) and the step number ( $n$ ) in the temperature cycle in the  $\text{O}_{x}\text{L}_y@z^n$  notation. We prepared the  $\text{O}_{226}\text{L}_{60}$  polymerization mixture in MeCN at  $[\text{VL}]_0 = 1$  M, corresponding to 36% (w/v) of the solid content (Table S3), and monitored the monomer consumption by in situ  $^1\text{H}$  NMR spectroscopy (Figure 3a) (see Figures S17–S23 for the full  $^1\text{H}$  NMR spectra). At 25 °C (denoted as  $\text{O}_{226}\text{L}_{60}@25^1$  in Figure 3), VL polymerization proceeded rapidly following pseudo-first-order kinetics with a  $k_p^{\text{app}}$  of  $0.07 \text{ min}^{-1}$  (Figure 3b) and reached a plateau of

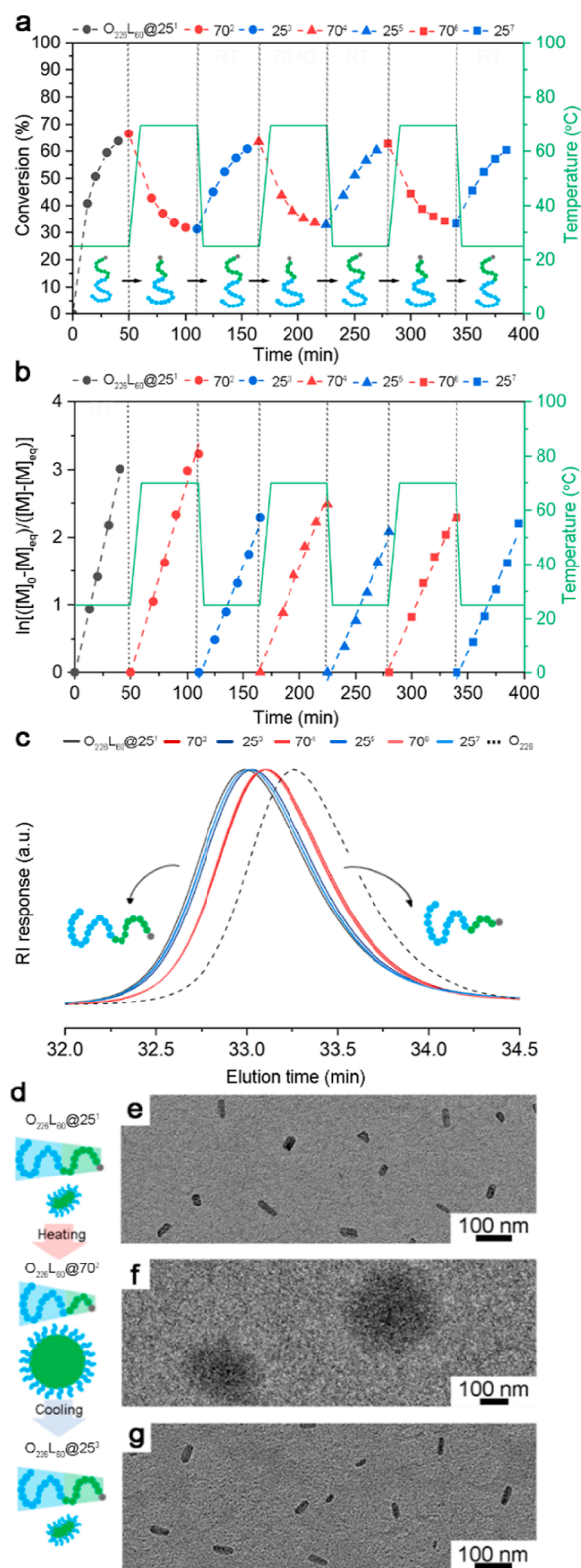


**Figure 3.** PDISA kinetics of  $\text{O}_{226}\text{L}_{60}$  in MeCN. (a) VL conversion during three successive temperature cycles of heating to 70 °C and cooling to 25 °C. (b) First-order kinetic plots. Note that  $[M]_0$  is given as the monomer concentration in the beginning of each step and  $[M]_{\text{eq}}$  varies as a function of temperature. (c) SEC traces. (d) Schematic representation of morphological transitions during PDISA. (e–g) Representative TEM images of  $\text{O}_{226}\text{L}_{60}@25^1$  (e),  $\text{O}_{226}\text{L}_{60}@70^2$  (f), and  $\text{O}_{226}\text{L}_{60}@25^3$  (g). Specimens were prepared by diluting the polymerization mixture to 3% concentration (w/v) using MeCN.

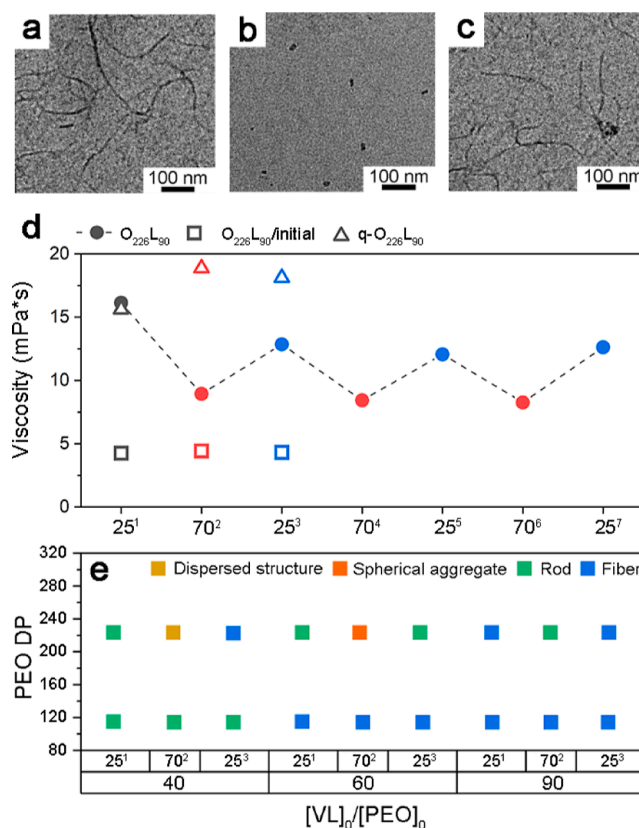
conversion at 67% within 50 min. Heating to 70 °C dropped the VL conversion by 31%, indicating depolymerization of PVL ( $O_{226}L_{60}@70^2$  in Figure 3). The ring-closing reaction at the propagating chain end seems to follow pseudo-first-order kinetics with a rate similar to that of the ring-opening reaction ( $k_{dp}^{app} = 0.06 \text{ min}^{-1}$ ). The VL conversion was recovered upon cooling to RT by polymerization but at a somewhat slower rate ( $O_{226}L_{60}@25^3$  in Figure 3,  $k_p^{app} = 0.04 \text{ min}^{-1}$ ). We observed that the depolymerization rate became identical to polymerization during the second heating cycle and the rate constant remained the same throughout the two additional temperature cycles. We posit that a trace impurity in the solution may slowly deactivate the TBD catalyst, decreasing the reaction rates in the first cycle. Then, the number of active catalytic species seems to be retained, providing a constant reaction rate. We also confirmed that adding more TBD during the temperature cycle can increase the rate.

Figure 3c shows how size exclusion chromatography (SEC) traces change during PDISA. After the heating and cooling, we quenched the polymerization mixture by adding acetic acid to kill the TBD catalyst (so the system becomes static) and analyzed the isolated polymer. A shift to a lower molar mass upon heating is consistent with the depolymerization of PVL. Cooling to RT restored the original trace of PEO-*b*-PVL nearly perfectly. The  $M_n$  value converges into 17.2–17.7 kg mol<sup>-1</sup> at 25 °C and 15.8–16.2 kg mol<sup>-1</sup> at 70 °C in equilibrium, accompanied by the change in VL conversion of 63–67% at 25 °C and 31–33% at 70 °C, strongly supporting the reversibility of polymerization/depolymerization processes at least for three cycles. Unimodal and narrow molar mass distributions [dispersity ( $\bar{D}$ ) < 1.15] were retained throughout the successive heating and cooling processes. After killing the catalyst, nearly no change in the molar mass was observed during the temperature cycle, indicating that the catalyst needs to be present in the solution to facilitate PDISA (Figures S24 and S25 and Table S4). We note that TBD has been reported to catalyze depolymerization of poly( $\gamma$ -butyrolactone).<sup>41</sup> Given that the ring-closing reaction also occurs via transesterification, it is reasonable that a polymerization catalyst for ring-opening (transesterification) polymerization can also catalyze depolymerization. Depolymerization and repolymerization could also be performed in DMSO (Figures S26–S30 and Tables S3 and S4). The depolymerization reaction in DMSO was much slower than MeCN, yet chain scission mediated by transesterification was noticeable upon prolonged heating.<sup>42–44</sup> Thus, depolymerization was performed at 120 °C for 1 h to accelerate the reaction with minimized transesterification. While the disappearance and regeneration of spherical micelles were observed during the temperature cycle consistent with the MeCN case, significant broadening in the molar mass distribution after heating and incomplete regeneration of the original molar mass upon cooling suggest that chain scission via intermolecular transesterification occurs to a noticeable extent in DMSO.

We found that the depolymerization and repolymerization processes accompanied abrupt morphological transitions (Figure 3d). We visualized the self-assembled morphologies using TEM and estimated the length of the observed objects by evaluating 100 particles in each image. Nanorods with an average length ( $L_n$ ) of  $41 \pm 9 \text{ nm}$ , initially formed after the VL polymerization at RT (Figure 3e), were transformed into larger, loose, and irregular spherical aggregates upon heating with the average diameter of  $154 \pm 53 \text{ nm}$  (Figure 3f). We

posit that the shortened PVL block by depolymerization becomes sparingly soluble in MeCN and forms loosely aggregated species. The nanorods with the  $L_n$  of  $43 \pm 8 \text{ nm}$ , composed of PEO corona chains grafted onto the crystalline PVL core,<sup>45</sup> were regenerated after cooling back to RT (Figure 3g) (see Figure S31 for statistical analysis). However, the quenched polymerization mixture at RT showed that the nanorod morphology persisted with the increasing rod length after the temperature cycle, which is likely a consequence of thermal annealing involving thinning of the crystalline core, dissolution of smaller particles upon heating, and lateral adhesion of unimers to remaining rods during cooling to grow further, as determined by TEM (Figure S32).<sup>46</sup>

We further explored morphological transitions in the PDISA process by varying the [VL]/[PEO] ratio and the PEO block length (Tables S3 and S4). When the [VL]/[PEO] ratio was increased to 90:1 (Figures S33–S35), the  $O_{226}L_{90}$  mixture produced much longer nanofibers after polymerization at RT ( $L_n = 276 \pm 55 \text{ nm}$ ) (Figure 4a). Depolymerization upon heating chops down the fibers and produces nanorods with  $L_n = 34 \pm 9 \text{ nm}$  (Figure 4b), which is similar to those obtained with the shorter PVL block shown in Figure 3.<sup>47</sup> Cooling to RT revives the nanofiber morphology, as evidenced by TEM (Figure 4c). We hypothesize that a change in the steric crowdedness of the PEO corona chains, which is inversely



**Figure 4.** (a–c) Representative TEM images of  $O_{226}L_{90}@25^1$  (a),  $O_{226}L_{90}@70^2$  (b), and  $O_{226}L_{90}@25^3$  (c). Specimens were prepared from MeCN solution with a concentration of 3% w/v solid. (d) Change in viscosity of the polymerization solution of  $O_{226}L_{90}$  during three temperature cycles of PDISA in MeCN, the solution of  $O_{226}L_{90}/\text{initial}$ , and  $q-O_{226}L_{90}$  during the first temperature cycle. (e) Phase diagram of micellar morphologies induced by PDISA in MeCN as a function of PEO DP, [PEO]/[VL] ratio, and temperature.



proportional to the contour length of the PVL block,<sup>26,48</sup> induces the observed morphological transition (see schematic illustration in Figure S36). The longer PVL block at RT reduces the steric hindrance between the PEO chains and promotes intercore fusion to produce long nanofibers. The increasing crowdedness in the PEO corona upon depolymerization splits the nanofiber into rods and relieves the congestion by repolymerization regenerates nanofibers with comparable lengths.

Interestingly, PDISA also induces macroscopic changes in the solution viscosity (Figure 4d and Table S5). Compared to the initial polymerization mixture, nanofiber formation by the VL polymerization jumps up the viscosity by three times accompanied by nanofiber formation. The viscosity is reduced by 50% upon heating of the solution to 70 °C, now consisting of shorter nanorods. In contrast, a RT-quenched O<sub>226</sub>L<sub>90</sub> (q-O<sub>226</sub>L<sub>90</sub>), an O<sub>226</sub>L<sub>90</sub> polymerization mixture without a catalyst (O<sub>226</sub>L<sub>90</sub>/initial), and MeCN do not show such a decrease in viscosity at 70 °C (nor an increase upon further cooling), indicating that depolymerization causes the viscosity drop. Repolymerizing VL upon cooling reconstructs the nanofiber and re-viscosifies the solution. The somewhat lower viscosity is almost restored to the initial level after equilibrating the solution at room temperature for 2 days. We demonstrate that the viscosity modulation can be repeated in at least three cycles with nearly perfect reproduction of VL conversion in <sup>1</sup>H NMR and SEC trace shifts (Figures S33 and S34). Again, no change in the molar mass or morphology was observed in the q-O<sub>226</sub>L<sub>90</sub> sample after heating and cooling (Figures S37–S39). To a comparable extent, a reduction in viscosity is also observed in O<sub>226</sub>L<sub>60</sub> (Figure S40). We posit that the amount of the polymeric species in the solution, rather than the morphological transition, would primarily affect the solution viscosity.

Figure 4e summarizes dominant morphologies produced via the PDISA process as a function of the [VL]/[PEO] ratio and the PEO block length (see Figures S41–S44 for the whole TEM data). In the case of the O<sub>226</sub>L<sub>40</sub> mixture with a decreased [VL]/[PEO] ratio of 40:1, the PVL block length seems too short to produce many micelles by polymerization. Depolymerization disassembles nearly all micelles, and repolymerization generates fibers rather than rods. We are still determining the origin of fiber formation. We did not observe depolymerization-induced morphological transitions with a shorter PEO block with a DP of 113.

## CONCLUSIONS

We established a PDISA strategy that allows us to adjust the chain length of the solvophobic block reversibly and thus control the packing parameter of the resulting block copolymer. The key was to choose a selective solvent whose solubility parameter is closest to that of the monomer but farthest from that of the polymer. Spontaneous micelle formation during the polymerization occurs, and the segregation of the solvophobic core from the reaction medium produces a noticeable entropic penalty toward polymerization. The entropy-driven depression of  $T_c$  is found as a result and facilitates control over the extent of polymerization in the relatively narrow temperature range.

We demonstrated the PDISA concept with the ROP of VL in the presence of hydroxyl-terminated PEO using TBD as a catalyst in MeCN. Elevating the temperature from RT to 70 °C facilitates depolymerization, leading to an ~40% reduction

in conversion. While diverse morphologies, including spherical aggregates, short nanorods, and long nanofibers, were found at RT depending on the initial [VL]/[PEO] ratio and PEO length, reversible morphological transitions, such as rod–sphere–rod and fiber–rod–fiber, could be achieved via PDISA during the heating and cooling cycles accompanied by changes in macroscopic properties such as viscosity. We envision PDISA as a useful tool for drastic viscosity reduction at higher temperatures if a depolymerization-induced morphological transition from entangled fibers to dispersed spheres can be realized.

Our results show that coupling polymerization equilibrium with self-assembly opens up new opportunities for manipulating polymerization. The PDISA approach will enrich the PISA toolbox and contribute to the development of new dynamic soft materials based on reversible polymerization. Utilizing advanced catalysts responsive to external stimuli such as light will add another dynamic feature to PDISA, allowing us to control polymerization and the corresponding morphological transition temporally.

## ASSOCIATED CONTENT

### Supporting Information

The Supporting Information is available free of charge at <https://pubs.acs.org/doi/10.1021/jacs.4c00612>.

Synthetic protocols and characterization data of PDISA of OLs by <sup>1</sup>H NMR, SEC, DSC, DLS, and TEM analyses; and viscosity measurement data (PDF)

## AUTHOR INFORMATION

### Corresponding Author

Myungeun Seo – Department of Chemistry, Korea Advanced Institute of Science and Technology (KAIST), Daejeon 34141, Republic of Korea; KAIST Institute for the Nanocentury, KAIST, Daejeon 34141, Republic of Korea; [orcid.org/0000-0002-5218-3502](https://orcid.org/0000-0002-5218-3502); Email: [seomyungeun@kaist.ac.kr](mailto:seomyungeun@kaist.ac.kr)

### Authors

Jiyeon Nam – Department of Chemistry, Korea Advanced Institute of Science and Technology (KAIST), Daejeon 34141, Republic of Korea; Present Address: Department of Chemistry, Colorado State University, Fort Collins, Colorado 80523, United States

Changsu Yoo – Department of Chemistry, Korea Advanced Institute of Science and Technology (KAIST), Daejeon 34141, Republic of Korea

Complete contact information is available at: <https://pubs.acs.org/10.1021/jacs.4c00612>

### Author Contributions

The manuscript was written through the contributions of all authors. All authors have given approval to the final version of the manuscript.

### Notes

The authors declare no competing financial interest.

## ACKNOWLEDGMENTS

This work was supported by the National Research Foundation of Korea (NRF) grant funded by the Korea government (MSIT) (2023R1A2C2005705 and 2018R1A5A1025208) and also by the Basic Science Research

Program through NRF funded by the Ministry of Education (2019R111A2A01063804).

## REFERENCES

- (1) Stupp, S. I.; LeBonheur, V.; Walker, K.; Li, L. S.; Huggins, K. E.; Keser, M.; Amstutz, A. Supramolecular Materials: Self-Organized Nanostructures. *Science* **1997**, *276*, 384–389.
- (2) Singer, S. J.; Nicolson, G. L. The Fluid Mosaic Model of the Structure of Cell Membranes. *Science* **1972**, *175*, 720–731.
- (3) Oda, T.; Iwasa, M.; Aihara, T.; Maeda, Y.; Narita, A. The Nature of the Globular- to Fibrous-Actin Transition. *Nature* **2009**, *457*, 441–445.
- (4) Pollard, T. D.; Borisy, G. G. Cellular Motility Driven by Assembly and Disassembly of Actin Filaments. *Cell* **2003**, *112*, 453–465.
- (5) Fortman, D. J.; Brutman, J. P.; De Hoe, G. X.; Snyder, R. L.; Dichtel, W. R.; Hillmyer, M. A. Approaches to Sustainable and Continually Recyclable Cross-Linked Polymers. *ACS Sustain. Chem. Eng.* **2018**, *6*, 11145–11159.
- (6) Jehanno, C.; Alty, J. W.; Roosen, M.; De Meester, S.; Dove, A. P.; Chen, E. Y. X.; Leibfarth, F. A.; Sardon, H. Critical Advances and Future Opportunities in Upcycling Commodity Polymers. *Nature* **2022**, *603*, 803–814.
- (7) Coates, G. W.; Getzler, Y. D. Y. L. Chemical Recycling to Monomer for an Ideal, Circular Polymer Economy. *Nat. Rev. Mater.* **2020**, *5*, 501–516.
- (8) Greer, S. C. Physical Chemistry of Equilibrium Polymerization. *J. Phys. Chem. B* **1998**, *102*, 5413–5422.
- (9) Dainton, F. S.; Ivin, K. J. Some Thermodynamic and Kinetic Aspects of Addition Polymerisation. *Q. Rev. Chem. Soc.* **1958**, *12*, 61–92.
- (10) Olsén, P.; Odelius, K.; Albertsson, A. C. Thermodynamic Presynthetic Considerations for Ring-Opening Polymerization. *Biomacromolecules* **2016**, *17*, 699–709.
- (11) Dainton, F.; Ivin, K. Reversibility of the Propagation Reaction in Polymerization Processes and its Manifestation in the Phenomenon of a ‘Ceiling Temperature’. *Nature* **1948**, *162*, 705–707.
- (12) Hocker, H.; Keul, H. Ring-Opening Polymerization and Ring-Closing Depolymerization. *Adv. Mater.* **1994**, *6*, 21–36.
- (13) Liu, H.; Nelson, A. Z.; Ren, Y.; Yang, K.; Ewoldt, R. H.; Moore, J. S. Dynamic Remodeling of Covalent Networks via Ring-Opening Metathesis Polymerization. *ACS Macro Lett.* **2018**, *7*, 933–937.
- (14) Zhou, L.; Zhang, Z.; Shi, C.; Scoti, M.; Barange, D. K.; Gowda, R. R.; Chen, E. Y. X. Chemically Circular, Mechanically Tough, and Melt-Processable Polyhydroxyalkanoates. *Science* **2023**, *380*, 64–69.
- (15) Brutman, J. P.; De Hoe, G. X.; Schneiderman, D. K.; Le, T. N.; Hillmyer, M. A. Renewable, Degradable, and Chemically Recyclable Cross-Linked Elastomers. *Ind. Eng. Chem. Res.* **2016**, *55*, 11097–11106.
- (16) Penfold, N. J. W.; Yeow, J.; Boyer, C.; Armes, S. P. Emerging Trends in Polymerization-Induced Self-Assembly. *ACS Macro Lett.* **2019**, *8*, 1029–1054.
- (17) Canning, S. L.; Smith, G. N.; Armes, S. P. A Critical Appraisal of RAFT-Mediated Polymerization-Induced Self-Assembly. *Macromolecules* **2016**, *49*, 1985–2001.
- (18) Lee, J.; Seo, M. Downsizing of Block Polymer-Templated Nanopores to One Nanometer via Hyper-Cross-Linking of High  $\chi$ -Low N Precursors. *ACS Nano* **2021**, *15*, 9154–9166.
- (19) Oh, T.; Cho, S.; Yoo, C.; Yeo, W.; Oh, J.; Seo, M. Polymerization-Induced Microphase Separation of a Polymerization Mixture into Nanostructured Block Polymer Materials. *Prog. Polym. Sci.* **2023**, *145*, 101738.
- (20) Blanazs, A.; Madsen, J.; Battaglia, G.; Ryan, A. J.; Armes, S. P. Mechanistic Insights for Block Copolymer Morphologies: How Do Worms Form Vesicles? *J. Am. Chem. Soc.* **2011**, *133*, 16581–16587.
- (21) Figg, C. A.; Simula, A.; Gebre, K. A.; Tucker, B. S.; Haddleton, D. M.; Sumerlin, B. S. Polymerization-Induced Thermal Self-Assembly (PITSA). *Chem. Sci.* **2015**, *6*, 1230–1236.
- (22) Pei, Y.; Lowe, A. B.; Roth, P. J. Stimulus-Responsive Nanoparticles and Associated (Reversible) Polymorphism via Polymerization Induced Self-Assembly (PISA). *Macromol. Rapid Commun.* **2017**, *38*, 1600528.
- (23) Deane, O. J.; Jennings, J.; Armes, S. P. Shape-Shifting Thermoreversible Diblock Copolymer Nano-Objects via RAFT Aqueous Dispersion Polymerization of 4-Hydroxybutyl Acrylate. *Chem. Sci.* **2021**, *12*, 13719–13729.
- (24) Blanazs, A.; Verber, R.; Mykhaylyk, O. O.; Ryan, A. J.; Heath, J. Z.; Douglas, C. W. I.; Armes, S. P. Sterilizable Gels from Thermoresponsive Block Copolymer Worms. *J. Am. Chem. Soc.* **2012**, *134*, 9741–9748.
- (25) Fielding, L. A.; Lane, J. A.; Derry, M. J.; Mykhaylyk, O. O.; Armes, S. P. Thermo-Responsive Diblock Copolymer Worm Gels in Non-Polar Solvents. *J. Am. Chem. Soc.* **2014**, *136*, 5790–5798.
- (26) Hurst, P. J.; Rakowski, A. M.; Patterson, J. P. Ring-opening polymerization-induced crystallization-driven self-assembly of poly-L-lactide-block-polyethylene glycol block copolymers (ROPI-CDSA). *Nat. Commun.* **2020**, *11*, 4690.
- (27) Grazon, C.; Salas-Ambrosio, P.; Ibarboure, E.; Buol, A.; Garanger, E.; Grinstaff, M. W.; Lecommandoux, S.; Bonduelle, C. Aqueous Ring-Opening Polymerization-Induced Self-Assembly (RO-PISA) of N-Carboxyanhydrides. *Angew. Chem., Int. Ed.* **2020**, *59*, 622–626.
- (28) Olsén, P.; Odelius, K.; Albertsson, A. C. Thermodynamic Presynthetic Considerations for Ring-Opening Polymerization. *Biomacromolecules* **2016**, *17*, 699–709.
- (29) Zhang, S.; Campagne, C.; Salaün, F. Influence of Solvent Selection in the Electrospraying Process of Polycaprolactone. *Appl. Sci.* **2019**, *9*, 402.
- (30) Paolucci, V.; D'Olimpio, G.; Lozzi, L.; Mio, A. M.; Ottaviano, L.; Nardone, M.; Nicotra, G.; Le-Cornec, P.; Cantalini, C.; Politano, A. Sustainable Liquid-Phase Exfoliation of Layered Materials with Nontoxic Polarclean Solvent. *ACS Sustain. Chem. Eng.* **2020**, *8*, 18830–18840.
- (31) Subrahmanyam, R.; Gurikov, P.; Dieringer, P.; Sun, M.; Smirnova, I. On the Road to Biopolymer Aerogels—Dealing with the Solvent. *Gels* **2015**, *1*, 291–313.
- (32) Saba, H.; Zhu, X.; Chen, Y.; Zhang, Y. Determination of Physical Properties for the Mixtures of [BMIM]Cl with Different Organic Solvents. *Chin. J. Chem. Eng.* **2015**, *23*, 804–811.
- (33) Ravikumar, V. R.; Schröder, A.; Köhler, S.; Çetinel, F. A.; Schmitt, M.; Kondrakov, A.; Eberle, F.; Eichler-Haeske, J. O.; Klein, D.; Schmidt-Hansberg, B.  $\gamma$ -Valerolactone: An Alternative Solvent for Manufacturing of Lithium-Ion Battery Electrodes. *ACS Appl. Energy Mater.* **2021**, *4*, 696–703.
- (34) Terada, M.; Marchessault, R. H. Determination of Solubility Parameters for Poly(3-Hydroxyalkanoates). *Int. J. Biol. Macromol.* **1999**, *25*, 207–215.
- (35) Adamska, K.; Voelkel, A. Hansen Solubility Parameters for Polyethylene Glycols by Inverse Gas Chromatography. *J. Chromatogr. A* **2006**, *1132*, 260–267.
- (36) Dainton, F. S.; Ivin, K. J. Reversibility of the Propagation Reaction in Polymerization Processes and its Manifestation in the Phenomenon of a ‘Ceiling Temperature’. *Nature* **1948**, *162*, 705–707.
- (37) Cederholm, L.; Wohler, J.; Olsén, P.; Hakkarainen, M.; Odelius, K. “Like Recycles Like”: Selective Ring-Closing Depolymerization of Poly(L-Lactic Acid) to L-Lactide. *Angew. Chem., Int. Ed.* **2022**, *61*, No. e202204531.
- (38) Olsén, P.; Undin, J.; Odelius, K.; Keul, H.; Albertsson, A. C. Switching from Controlled Ring-Opening Polymerization (CROP) to Controlled Ring-Closing Depolymerization (CRCDP) by Adjusting the Reaction Parameters That Determine the Ceiling Temperature. *Biomacromolecules* **2016**, *17*, 3995–4002.
- (39) Price, C. Micelle Formation by Block Copolymers in Organic Solvents. *Pure Appl. Chem.* **1983**, *55*, 1563–1572.
- (40) Pan, A.; Rakshit, A. K.; Moulik, S. P. Micellization Thermodynamics and the Nature of Enthalpy-Entropy Compensation. *Colloids Surf., A* **2016**, *495*, 248–254.

- (41) Hong, M.; Chen, E. Y. X. Completely Recyclable Biopolymers with Linear and Cyclic Topologies via Ring-Opening Polymerization of  $\gamma$ -Butyrolactone. *Nat. Chem.* **2016**, *8*, 42–49.
- (42) Jehanno, C.; Pérez-Madrigal, M. M.; Demarteau, J.; Sardon, H.; Dove, A. P. Organocatalysis for Depolymerisation. *Polym. Chem.* **2019**, *10*, 172–186.
- (43) Leibfarth, F. A.; Moreno, N.; Hawker, A. P.; Shand, J. D. Transforming Polylactide into Value-Added Materials. *J. Polym. Sci., Part A: Polym. Chem.* **2012**, *50*, 4814–4822.
- (44) Meimoun, J.; Favrelle-Huret, A.; Winter, J. D.; Zinck, P. Poly(L-Lactide) Epimerization and Chain Scission in the Presence of Organic Bases. *Macromolecules* **2022**, *2*, 236–246.
- (45) Ren, Y.; Wei, Z.; Wu, T.; Bian, Y.; Leng, X.; Zhou, C.; Li, Y. Synthesis of Highly Branched Poly( $\delta$ -Valerolactone)s: A Comparative Study between Comb and Linear Analogues. *RSC Adv.* **2016**, *6*, 45791–45801.
- (46) Guerin, G.; Rupar, P.; Molev, G.; Manners, I.; Jinnai, H.; Winnik, M. A. Lateral Growth of 1D Core-Crystalline Micelles upon Annealing in Solution. *Macromolecules* **2016**, *49*, 7004–7014.
- (47) Hwang, S. H.; Kang, S. Y.; Yang, S.; Lee, J.; Choi, T. L. Synchronous Preparation of Length-Controllable 1D Nanoparticles via Crystallization-Driven in Situ Nanoparticlization of Conjugated Polymers. *J. Am. Chem. Soc.* **2022**, *144*, 5921–5929.
- (48) Vilgis, T.; Halperin, A. Aggregation of Coil-Crystalline Block Copolymers: Equilibrium Crystallization. *Macromolecules* **1991**, *24*, 2090–2095.